Int. J. Multiphase Flow Vol. 17, No. 4, pp. 469–483, 1991
Printed in Great Britain

0301-9322/91 $3.00 + 0.00
Pergamon Press/Elsevier

DYNAMIC VISCOUS RESUSPENSION

B. K. CHAPMAN and D. T. LEIGHTON JR
Department of Chemical Engineering, University of Notre Dame, Notre Dame, IN 46556, U.S.A.

(Received 15 April 1990; in revised form 19 February 1991)

Abstract—The resuspension of a settled layer of particles under viscous flow conditions has been attributed to shear-induced dispersion processes arising from the interaction between particles as a suspension is sheared. Previous studies were confined to steady-state measurements of the height of a resuspending layer as a function of applied shear stress. In this paper we present dynamic measurements of the response of a suspension of negatively buoyant non-colloidal spheres to a step change in the applied shear rate. The time-dependent variation in observed viscosity is used to estimate the shear-induced effective diffusivity within the plane of shear and the hindered settling factor in sheared suspensions at concentrations between 20 and 50% by volume.

Key Words: viscous resuspension, shear-induced migration, hindered settling

1. INTRODUCTION

Resuspension is a process whereby a settled layer of negatively buoyant spheres, in the presence of a shear flow, becomes entrained in the bulk fluid. While resuspension has typically been associated with high Reynolds number flows or turbulence (Thomas 1961), recently it has been shown to also occur at sufficiently low Reynolds numbers such that laminar conditions exist and inertial effects are insignificant (Gadala-Maria 1979; Leighton & Acrivos 1986).

The resuspension of a settled layer of particles under viscous flow conditions was indirectly observed by Gadala-Maria (1979) while studying the rheological properties of suspensions of 50 μm coal particles in viscous Newtonian fluids with a parallel-plate device. Gadala-Maria found that after allowing the suspension to rest overnight, the coal particles, being negatively buoyant, settled out. This resulted in a lower viscosity initially observed upon the application of shear. Subsequently, however, provided a sufficient level of shear was applied to the suspension, the viscosity would gradually increase and attain the previous day's steady-state value. This increase was attributed to the resuspension of the coal particles.

In a more complete investigation of this phenomenon, Leighton & Acrivos (1986) showed that the viscous resuspension of a settled layer of particles could be described in terms of a shear-induced diffusion process (Leighton & Acrivos 1987b), in which the diffusivity arose from the interaction between the particles as the suspension was sheared. Since the rate of interparticle interactions is proportional to the shear rate $\dot{\gamma}$ and the resulting displacement across steamlines scales with the particle radius a, the effective diffusivity from interactions is proportional to $\dot{\gamma}a^2$. This phenomenon has been observed in Couette viscometers and in Poiseuille flows (Leighton & Acrivos 1987b). It is quite different from the conventional Brownian diffusivity that arises from molecular motion and which, for spherical particles, is given by

$$D_B = \frac{kT}{6\pi\mu a} \qquad [1]$$

for a dilute suspension. The ratio between these diffusivities scales as the Peclet number, $\mathrm{Pe} = \dot{\gamma}\mu a^3/kT$, which for typical viscous resuspension experiments is of the order of 10^8. This phenomenon is also distinct from inertial lift mechanisms (Segre & Silberberg 1962a, b; Ho & Leal 1974), in which the dispersive forces are due to the inertia of the suspending phase. Typical particle Reynolds numbers for viscous resuspension experiments are of the order of 10^{-4}, for which inertial forces should be negligible.

It should be noted that the shear-induced effective diffusivity (or gradient diffusivity) is quite different from the shear-induced coefficient of self-diffusion. Shear-induced self-diffusion, investigated experimentally by Leighton & Acrivos (1987a) and Eckstein *et al.* (1977) and via numerical simulation by Bossis & Brady (1987), arises from the random motion of the particles which occurs as they tumble over one another in a shear flow. Thus, self-diffusion governs the mixing of labeled particles in a sheared suspension at a uniform concentration. In contrast, the gradient or effective diffusivity is defined as the ratio of the particle flux resulting from a concentration gradient to the magnitude of the gradient. Since the interaction of particles in a sheared suspension may act to "push" particles from regions of high concentration to low, the effective diffusivity is not necessarily the result of a random walk process, and may be much greater than the coefficient of self-diffusion. Leighton & Acrivos (1987a, b) have demonstrated that the shear-induced effective diffusivity is nearly an order of magnitude greater than the coefficient of self-diffusion at a concentration of 40% by vol.

Leighton & Acrivos modeled the resuspension process as a balance between the downward flux of particles due to sedimentation and an upward flux due to a shear-induced effective diffusion along concentration gradients. At steady state this balance resulted in an expansion in the height of an initially settled bed whose magnitude was proportional to an integral of the effective diffusivity, and also to the Shields parameter $\Phi = \tau/\Delta\rho g a$. The Shields parameter is the ratio of viscous forces to gravitational forces, where τ is the applied shear stress and $\Delta\rho g$ is the buoyancy force. A similar model was employed by Schaflinger *et al.* (1990) to describe the viscous transport of sedimenting spheres in pressure-driven channel flow, and by Davis & Leighton (1987) for transport in cross-flow microfiltration devices. These authors obtained reasonable agreement between measured suspension heights and integrals of the effective diffusivity measured in independent experiments (Leighton & Acrivos 1987b), however no transient experiments were carried out.

In this paper we focus on the dynamic response of a partially resuspended suspension to a step change in the applied shear rate. In section 2 we show how the concentration distribution is related to the applied shear rate and determine its effect on the apparent viscosity of the suspension. In section 3 we describe our experiments, in which we subject a suspension to a step increase and decrease in shear rate and measure the resulting transient torque signal. In section 4 we use these measurements to determine the effective diffusivity within the plane of shear over a much wider range of concentration than previously reported in the literature. We also calculate the hindered settling factor, f, for a suspension in the plane of shear. Previous measurements of the hindered settling factor have been made for unsheared suspensions, or those settling normal to the plane of shear (Lynch 1985). In the final section we summarize our results and compare the measured diffusivity with values previously reported in the literature.

2. THEORY

2.1. Steady-state analysis

Consider a suspension of negatively buoyant spheres undergoing shear in the plane Couette flow depicted in figure 1. Physically, such a flow may be produced by an annular parallel-plate viscometer—essentially a parallel-plate viscometer with the center removed. At steady state the concentration distribution of the particles will be governed by a balance between the settling velocity of the particles and a shear-induced diffusive flux. In this study the gravitational vector is parallel to the velocity gradient. Following Leighton & Acrivos (1986), the volumetric particle flux N_y is given by

$$N_y = -\frac{2}{9}\frac{\Delta\rho g a^2}{\mu_0} f\phi - D_{\|}\frac{\mathrm{d}\phi}{\mathrm{d}y}, \qquad [2]$$

where ϕ is the volume fraction of particles, f is the hindrance to settling caused by the presence of other particles, μ_0 is the viscosity of the pure suspending fluid, a is the particle radius, $g\ \Delta\rho$ is the buoyancy force and $D_{\|}$ is the shear-induced effective diffusivity within the plane of shear. At steady

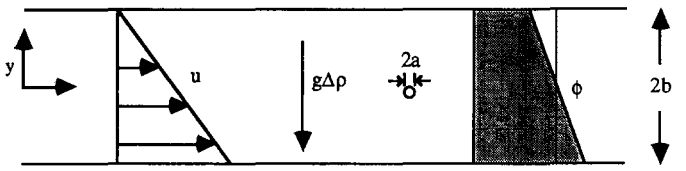

Figure 1. The flow field. Rotation of the lower annular plate results in a shear flow. Shear-induced dispersion balances sedimentation and produces a steady-state concentration profile. The relative particle size indicated its approximately that used in a typical experiment.

state, recalling that the effective diffusivity is proportional to the shear rate $\dot{\gamma} = \tau/(\mu_r u_0)$ where μ_r is the relative viscosity of the suspension, we obtain

$$\frac{d\phi}{dy^*} = -\frac{2}{9}\left(\frac{b}{a}\right)\left(\frac{\Delta\rho g a}{\tau}\right)\left(\frac{f\phi\mu_r}{\hat{D}_\parallel}\right), \qquad [3]$$

where we have rendered y dimensionless with respect to half of the gap height b, and $\hat{D}_\parallel = D_\parallel/(\dot{\gamma}a^2)$ is the dimensionless effective diffusivity. Note that the dimensionless concentration gradient is inversely proportional to both the particle size to gap height ratio a/b and the Shields parameter $\Psi = (\tau/\Delta\rho g a)$. The quantity $[(f\phi\mu_r)/\hat{D}_\parallel]$ was determined in the course of the experiments described in the next section (cf. figure 9) to be a weak function of concentration (at least in comparison with the viscosity and diffusivity) over the range of concentrations examined here. For sufficiently large values of Ψ and a/b the concentration variation across the gap will be small, hence the quantity $[(f\phi\mu_r)/\hat{D}_\parallel]$ will be nearly constant in the gap and the concentration profile will be approximately linear. In the experiments described in section 3 we examine suspension characteristics as a function of $\Psi a/b$ and determine the asymptotic behavior as $\Psi a/b$ becomes large.

Of particular importance is the effect of the concentration profile on the observed viscosity. For the simple flow considered here, the reciprocal of the observed viscosity is given by

$$\frac{1}{\mu_{r,obs}} = \frac{1}{2b}\int_{-b}^{b}\frac{1}{\mu_r}\,dy. \qquad [4]$$

If we expand the function $1/\mu_r$ in a Taylor series about $\phi = \bar{\phi}$, the average concentration in the gap, we obtain

$$\frac{1}{\mu_r} = \frac{1}{\mu_r}\bigg|_{\bar{\phi}} + \frac{\partial\left(\frac{1}{\mu_r}\right)}{\partial\phi}\bigg|_{\bar{\phi}}(\phi-\bar{\phi}) + \frac{1}{2}\frac{\partial^2\left(\frac{1}{\mu_r}\right)}{\partial\phi^2}\bigg|_{\bar{\phi}}(\phi-\bar{\phi})^2 + O[(\phi-\bar{\phi})^3]. \qquad [5]$$

Substituting into [4] and noting that the average of $(\phi - \bar{\phi})$ across the gap is zero, we obtain

$$\frac{\mu_r|_{\bar{\phi}}}{\mu_{r,obs}} - 1 = \frac{1}{2}\left[\mu_r\frac{\partial^2\left(\frac{1}{\mu_r}\right)}{\partial\phi^2}\right]\bigg|_{\bar{\phi}}\langle(\Delta\phi)^2\rangle + O\langle(\Delta\phi)^3\rangle, \qquad [6]$$

where $\Delta\phi$ is the deviation from the average concentration and angle brackets denote an average over the gap. Thus, for small concentration gradients, the viscosity function $(\mu_r|_{\bar{\phi}}/\mu_{r,obs} - 1)$ is proportional to the mean square concentration fluctuation. Note that the viscosity function in [6] involves the second derivative of $1/\mu_r$. We found in our experiments that the reciprocal of the relative viscosity was very nearly a quadratic function of concentration (cf. figure 6) and that the second derivative of the function was positive. This means any fluctuation in concentration across the gap results in a decrease in the observed viscosity. Because the reciprocal of the relative viscosity was nearly quadratic, neglecting higher-order terms in [6] is a reasonable approximation even for relatively large concentration gradients.

If we assume that our concentration profile is linear, then

$$\Delta\phi = -\frac{2}{9}\left(\frac{b}{a}\right)\left(\frac{\Delta\rho g a}{\tau}\right)\left(\frac{f\phi\mu_r}{\hat{D}_\parallel}\right)\bigg|_{\phi=\bar{\phi}}\frac{y}{b}, \qquad [7]$$

and hence the mean square concentration deviation is given by

$$\langle(\Delta\phi)^2\rangle = \frac{1}{3}\left\{\frac{2}{9}\left(\frac{b}{a}\right)\left(\frac{\Delta\rho g a}{\tau}\right)\left(\frac{f\phi\mu_r}{\hat{D}_\parallel}\right)\bigg|_{\phi=\bar{\phi}}\right\}^2. \quad [8]$$

For a given applied shear stress τ and average concentration $\bar{\phi}$, the deviation between the observed viscosity and that at a uniform concentration is thus given by

$$\frac{\mu_r|_{\bar{\phi}}}{\mu_{r,obs}} - 1 = \frac{1}{2}\mu_r \frac{\partial^2\left(\frac{1}{\mu_r}\right)}{\partial\phi^2}\bigg|_{\bar{\phi}} \frac{1}{3}\left\{\frac{2}{9}\left(\frac{b}{a}\right)\left(\frac{\Delta\rho g a}{\tau}\right)\left(\frac{f\phi\mu_r}{\hat{D}_\parallel}\right)\bigg|_{\phi=\bar{\phi}}\right\}^2. \quad [9]$$

Equation [9] provides a relation between the product of the Shields parameter and particle size and the effective diffusivity and hindered settling factor. From steady-state experiments, a plot of this viscosity deviation vs $[b/(a\Psi)]^2$ will thus yield the ratio of the hindered settling factor f to the effective diffusivity, $\hat{D}_\parallel$. To evaluate $\hat{D}_\parallel$ independently, however, we will examine the transient response of a suspension to a step change in shear.

2.2. *Transient analysis*

When a suspension is subjected to a step increase in shear, we expect the concentration profile between the two plates to become more uniform though an increase in the effective diffusivity. Because of the observed dependence of viscosity on concentration, this will lead to an increase in the measured torque and thus the observed viscosity. The time-dependent concentration distribution is governed by

$$\frac{\partial\phi}{\partial t} = \frac{\partial}{\partial y}\left(\frac{2}{9}\frac{\Delta\rho g a^2}{\mu_0} f\phi + D_\parallel \frac{\partial\phi}{\partial y}\right), \quad [10]$$

which, due to the dependence of viscosity, diffusivity and the hindered settling factor on concentration, is highly non-linear. To obtain an analytic solution to [10] we shall limit ourselves to cases of small gradients in concentration which result from large values of $\Psi a/b$. With this approximation, we assume f and $D_\parallel$ are approximately constant within the gap and [10] reduces to

$$\frac{\partial\phi}{\partial t} = D_\parallel \frac{\partial^2\phi}{\partial y^2} \quad [11]$$

with the no flux boundary conditions $N_y = 0$ at $y = \pm b$. Using [3], the boundary conditions may be rewritten as

$$\frac{d\phi}{dy^*}\bigg|_{y^*=\pm 1} = -\frac{2}{9}\left(\frac{1}{\Psi_H \frac{a}{b}}\right)\left(\frac{f\phi\mu_r}{\hat{D}_\parallel}\right) \equiv -\delta, \quad [12]$$

where Ψ_H is the Shields parameter at the higher applied shear and $y^* = y/b$. For a constant applied shear rate, changes in the observed viscosity will result in changes in the Shields parameter Ψ_H and hence in the concentration gradient δ. For small concentration gradients, however, the variation in the viscosity will be small and hence Ψ_H and δ will be approximately constant in time.

Before application of the step increase in shear the suspension will have the steady-state concentration distribution corresponding to the lower applied shear stress. Again, for small concentration gradients, we obtain the initial linear profile

$$\phi - \bar{\phi} = -\frac{2}{9}\left(\frac{1}{\Psi_L \frac{a}{b}}\right)\left(\frac{f\phi\mu_r}{\hat{D}_\parallel}\right) y^* = -(\alpha + \delta)y^*, \quad [13]$$

where Ψ_L is the Shields parameter corresponding to the initial shear. The initial concentration gradient $\alpha + \delta$ is assumed to be constant across the gap.

The ratio of the initial and final concentration gradients is simply the ratio of the applied shear rates, i.e.

$$\frac{\alpha+\delta}{\delta}=\frac{\dot{\gamma}_H}{\dot{\gamma}_L}. \qquad [14]$$

With this relationship, the time-dependent concentration profile is given by

$$\phi(t^*,y^*)-\bar{\phi}=y^*\delta+\sum_{n=0}^{\infty}\frac{2\alpha(-1)^n}{(n+\frac{1}{2})^2\pi^2}\sin[(n+\tfrac{1}{2})\pi y^*]\exp[-(n+\tfrac{1}{2})^2\pi^2\hat{D}_\parallel t^*], \qquad [15]$$

where $t^*=t\dot{\gamma}_H a^2/b^2$. Noting that $\phi(t^*,y^*)-\bar{\phi}$ is $\Delta\phi$, we may obtain an expression for $\langle(\Delta\phi)^2\rangle$ by squaring [15] and integral averaging each term from $y^*=-1$ to $y^*=1$:

$$\langle(\Delta\phi)^2\rangle=\frac{\delta^2}{3}+\sum_{n=0}^{\infty}\frac{4\alpha\,\delta}{(n+\frac{1}{2})^4\pi^4}\exp[-(n+\tfrac{1}{2})^2\pi^2\hat{D}_\parallel t^*]$$

$$+\sum_{n=0}^{\infty}\frac{2\alpha^2}{(n+\frac{1}{2})^4\pi^4}\exp[-2(n+\tfrac{1}{2})^2\pi^2\hat{D}_\parallel t^*]; \qquad [16]$$

and hence the time-dependent viscosity is given by

$$\frac{\mu_r|_{\bar{\phi}}}{\mu_{r,obs}}-1=\frac{1}{2}\left[\mu_r\frac{\partial^2\left(\frac{1}{\mu_r}\right)}{\partial\phi^2}\right]\Bigg|_{\bar{\phi}}\left\{\frac{\delta^2}{3}+\sum_{n=0}^{\infty}\frac{4\alpha\,\delta}{(n+\frac{1}{2})^4\pi^4}\exp[-(n+\tfrac{1}{2})^2\pi^2\hat{D}_\parallel t^*]\right.$$

$$\left.+\sum_{n=0}^{\infty}\frac{2\alpha^2}{(n+\frac{1}{2})^4\pi^4}\exp[-2(n+\tfrac{1}{2})^2\pi^2\hat{D}_\parallel t^*]\right\}. \qquad [17]$$

The relative viscosity at $t=0$ is given by

$$\frac{\mu_r|_{\bar{\phi}}}{\mu_{r,obs}|_{t=0}}-1=\frac{1}{2}\left(\mu_r\frac{\partial^2\left(\frac{1}{\mu_r}\right)}{\partial\phi^2}\right)\Bigg|_{\bar{\phi}}\frac{(\alpha+\delta)^2}{3}. \qquad [18]$$

Substituting [18] into [17] we obtain an expression for the time-dependent change in the dimensionless observed viscosity:

$$\frac{\frac{\mu_r|_{\bar{\phi}}}{\mu_{r,obs}}-1}{\frac{\mu_r|_{\bar{\phi}}}{\mu_{r,obs}|_{t=0}}-1}=\left\{\frac{\left(\frac{\delta}{\alpha}\right)^2}{\left(1+\frac{\delta}{\alpha}\right)^2}+\sum_{n=0}^{\infty}\frac{12\frac{\delta}{\alpha}}{\left(1+\frac{\delta}{\alpha}\right)^2\left(n+\frac{1}{2}\right)^4\pi^4}\exp[-(n+\tfrac{1}{2})^2\pi^2\hat{D}_\parallel t^*]\right.$$

$$\left.+\sum_{n=0}^{\infty}\frac{6}{\left(1+\frac{\delta}{\alpha}\right)^2\left(n+\frac{1}{2}\right)^4\pi^4}\exp[-2(n+\tfrac{1}{2})^2\pi^2\hat{D}_\parallel t^*]\right\}. \qquad [19]$$

We may determine α, δ and $\mu_r|_{\bar{\phi}}$ from the measured initial and steady-stage viscosities and the relationship between α, δ and the applied shear rates given by [14]. Note that the transient behavior depends only on the diffusivity and the ratio δ/α, e.g. not on the absolute magnitude of the calculated concentration gradient. Diffusivities obtained by fitting [19] to transient viscosity measurements are thus unaffected by errors in measuring $1/\mu_r$ and its second derivative. In the limit

that $\delta/\alpha \ll 1$ (a condition present during our experiments) and noting that $\mu_{r,obs}$ at $t = \infty$ is approximately $\mu_r|_{\bar{\phi}}$, [19] simplfiies to

$$\frac{\dfrac{\mu_{r,obs}|_{t=\infty}}{\mu_{r,obs}} - 1}{\dfrac{\mu_{r,obs}|_{t=\infty}}{\mu_{r,obs}|_{t=0}} - 1} \approx \sum_{n=0}^{\infty} \frac{6}{\left(n + \frac{1}{2}\right)^4 \pi^4} \exp[-2(n + \tfrac{1}{2})^2 \pi^2 \hat{D}\ t^*], \quad [20]$$

which is solely a function of the dimensionless diffusivity. This emphasizes the fact that the calculation of the diffusivity depends only on the rate at which the viscosity approaches steady state. For the parameters used in our experiments the diffusivity calculated using [20] was only about 15% less than that calculated using [19]. The corresponding transient in the observed viscosity for a step decrease in shear is given in [21]:

$$\frac{\dfrac{\mu_r|_{\bar{\phi}}}{\mu_{r,obs}} - 1}{\dfrac{\mu_r|_{\bar{\phi}}}{\mu_{r,obs}|_{t=\infty}} - 1} = 1 - \sum_{n=0}^{\infty} \frac{12}{\left(1 + \frac{\delta}{\alpha}\right)\left(n + \frac{1}{2}\right)^4 \pi^4} \exp[-(n + \tfrac{1}{2})^2 \pi^2 \hat{D}\ t^*] + \sum_{n=0}^{\infty} \frac{6}{\left(1 + \frac{\delta}{\alpha}\right)^2 \left(n + \frac{1}{2}\right)^4 \pi^4} \exp[-2(n + \tfrac{1}{2})^2 \pi^2 \hat{D}\ t^*], \quad [21]$$

where t^* has now been rendered dimensionless with γ_L rather than γ_H.

It is interesting to note that the characteristic strains at which the steady-state viscosity is achieved for a step increase and decrease in shear are different. Since $\alpha \gg \delta$ (e.g. $\gamma_H \gg \gamma_L$), we expect the third term in [19] to dominate the transient in the observed viscosity for a step increase at large times, and the second term in [21] to dominate for a step decrease. Examination of the exponents in these terms reveals that the steady-state viscosity should be achieved twice as rapidly (where time is normalized by the shear rate) for a step increase in the shear rate as would be found for a step decrease. This discrepancy arises from the non-linear dependence of viscosity on the concentration profile.

From the determination of $\hat{D}$ in these experiments, it is possible to calculate the hindered settling coefficient, f, in the plane of shear. From [2] and noting at steady state under the low shear rate condition that

$$\frac{d\phi}{dy} = -\frac{(\alpha + \delta)}{b}, \quad [22]$$

we may obtain an expression for f:

$$f = \frac{9}{2} \frac{\mu_0 \dot{\gamma}_L}{\Delta \rho g \phi} \hat{D}\ \frac{(\alpha + \delta)}{b}. \quad [23]$$

It is important to note that the preceding equations have been derived assuming that the concentration variation across the gap is sufficiently small that variations in $\hat{D}$, f and μ_r may be neglected. This, of course, will be justified in the limit $\Psi_L a/b \gg 1$, since the characteristic concentration gradient is inversely proportional to this parameter. We may use our experiments to judge the validity of this approximation by calculating $\hat{D}$ and f as a function of $\Psi_L a/b$ and examining their asymptotic behavior as $\Psi_L a/b$ becomes large.

3. EXPERIMENTAL WORK

3.1. Materials

Particles used in the experiments consisted of two size ranges of glass spheres and one size of polystyrene spheres. The glass spheres were two lots of Class V-A microbeads obtained from Ferro

Corp. Cataphote Div., one of size 45–53 μm dia and one size 106–125 μm dia. Both lots were reported to be 90% in the listed size range. These spheres were dry sieved in order to increase the percentage of true spheres within each lot and to tighten the size distribution. The diameters of 100 particles of each lot size were measured optically. The area-averaged size distributions of the large spheres and the small spheres were 110.3 ± 13.6 and 46.7 ± 5.2 μm dia, respectively, where the error given is the 1σ population standard deviation (a measure of the width of the size distribution) rather than the error in the mean. Area-averaged distributions were calculated because of the relationship of the particle radius to the diffusivity.

The glass particles were suspended in an 88 wt% solution of glycerin and water. The density of the large spheres was measured via water displacement and found to agree with the reported value of 2.42 g/cm^3. The glycerin–water solution had a density of 1.23 g/cm^3, thus the large spheres had a density difference of 1.19 g/cm^3. While the density of the small glass spheres was also reported to be 2.42 g/cm^3, it was measured to be 2.34 g/cm^3. The deviation in the densities between the two size lots was probably due to the larger volume percentage of air bubbles in the small spheres. The viscosity of the suspending fluid was measured as a function of temperature on a CarriMed controlled stress rheometer and had a value of 1.62 P at 23.0°C. The temperature dependence of the pure fluid viscosity was important for accurate calculation of the hindered settling factor and the suspension relative viscosity.

The polystyrene spheres were reclaimed from the experiments of Leighton & Acrivos (1986, 1987b) and had a number-averaged mean diameter of 46.0 ± 2.6 μm (Leighton & Acrivos 1987b). These particles enabled direct comparison with earlier measurements of the diffusivity in the plane of shear. The spheres were suspended in the lubricant SF1147, a silicone oil obtained from General Electric. The density of the polystyrene spheres were reported to be 1.051 g/cm^3, while the SF1147 had a reported density of 0.887 g/cm^3, yielding a density difference of 0.163 g/cm^3. The viscosity of the suspending fluid was also measured as a function of temperature and had a value of 0.63 P at 23.0°C.

The suspensions were analyzed using an annular parallel-plate viscometer, with 19.05 cm o.d. and 14.05 cm i.d. yielding an aspect ratio of $(R_o - R_i)/\bar{R} = 0.302$. This geometry yielded a shear stress which had a radial deviation from that at the average radius $\bar{R}$ of $\pm 15\%$. The annular plates were mounted on a model R-18 Weissenberg Rheogoniometer equipped with a special clutch which allowed for switching between two drive motors operating at different rotational speeds. This clutch system resulted in a nearly instantaneous step change in shear rate.

3.2. Procedure

Well-mixed suspensions were loaded in the annular parallel-plate viscometer by carefully pouring them around the surface of the lower plate. The upper plate was then lowered slowly until it contacted the suspension. When contact between the suspension and the upper plate was completed over 360°, the plate was lowered further until the gap between the plates was completely filled. By slowly rotating the bottom plate during the lowering of the upper plate and by placing a thin layer of Vaseline on the outer and inner edges of the plates, the leakage of suspension was lessened, particularly in the glycerin–water systems. Through the rotation of the lower plate, a shear flow was produced in the gap between the lower and upper plates. The resultant torque on the upper plate was measured through the use of a transducer and a chart recorder. The observed relative viscosity was taken to be the ratio of the torque measured for a suspension to that measured for the pure suspending fluid in the same device with corrections for temperature and shear rate variations. In this way, most sources of systematic error in relative viscosity measurement were eliminated from the experiments.

Viscous resuspension was studied over a wide range of experimental conditions. Suspensions of large glass spheres were studied over concentrations from 20 to 50%. The small glass sphere suspensions were limited to studies at 40.9 , 45.9 and 50.9%, primarily due to the excessively long time necessary to approach steady state at lower concentrations. The polystyrene suspensions were only examined at 45 and 50% because of leaking problems associated with the low viscosities at lower concentrations and the strong ability of the suspending fluid to wet the plate surfaces.

The gap heights used for each experiment ranged from 0.88 to 2.8 mm. This resulted in particle diameter to gap height ratios ranging from 0.020 to 0.093. For larger gaps, the suspensions had a tendency to leak out the edges of the plates, therefore most experiments were performed at gaps of <2.5 mm. A typical set of experiments was started at a small gap height and, at completion, the upper plate was raised and additional suspension was added to slightly increase the gap height for a new set of experiments. This was repeated until the gap heights approached 2.8 mm.

Suspensions were sheared at rates ranging from 0.6 to 190 s^{-1}, depending on the concentration of the suspension. In general, as suspension concentration decreased (and hence the diffusivity as well), a higher shear rate was necessary to achieve resuspension. These shear rates gave rise to Shields parameters in the range of 6.7–466, which were sufficient to lead to a nearly uniform concentration profile at high shear and to avoid settling at low shear. The step changes in shear were by factors of $10^{0.7}$–$10^{1.4}$. These changes were adjusted to keep α and δ within acceptable parameter ranges. Several experiments were conducted at considerably lower shear rates ($\Psi \approx 2$ to 7 for the 40% large glass sphere suspensions as opposed to 12–25 for the diffusivity measurement experiments) to examine the response of a settled bed to a step change in shear. These experiments were not used to estimate either the diffusivity or hindered settling factor as they lay well outside the range of parameters where [19] and [21] would be valid. The temperature was monitored frequently during each experiment through the use of a digital thermometer with a probe attached to the top surface of the upper plate.

4. RESULTS

4.1. General observations

Upon increasing the shear rate imposed on a suspension which is at steady state at lower shear, the observed torque signal increased nearly instantaneously (<0.25 s) to reflect the torque produced at the viscosity corresponding to the initial concentration profile. Upon further shearing, the concentration within the gap became more uniform, resulting in a gradually increasing torque signal. This continued until the suspension reached steady state at the higher shear rate. The opposite effect was seen with a step decrease in shear rate.

The time required to reach steady state generally increased in experiments with smaller particles and concentrations. This was the result of the influence of particle radius and concentration on the effective diffusivity. In addition, as expected from the model, step decrease experiments took much longer than step increase experiments to reach steady state. For instance, in a 45% large glass sphere suspension a step increase experiment would reach steady state in approx. 15 s, while a step decrease experiment—conducted at an order of magnitude lower shear rate—took on the order of 5 min. When typical observed viscosity measurements for each type of experiment are plotted vs

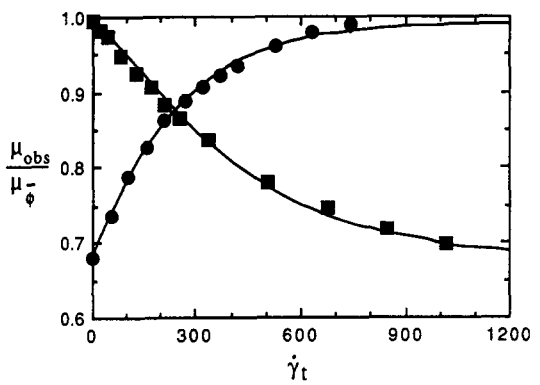

Figure 2. Comparison of step increase and step decrease viscosity variation. Data for a 40% suspension of 106–125 μm glass spheres: ■, step decrease $\hat{D}_\parallel = 0.451$; ●, step increase $\hat{D}_\parallel = 0.488$. Note that the characteristic strain for a step decrease experiment is greater, as expected from theory. The solid lines are [19] and [21] fitted to the data.

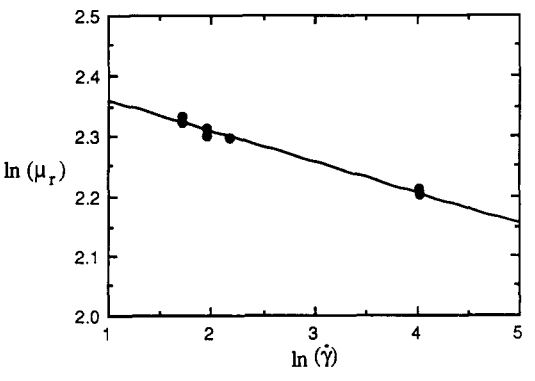

Figure 3. The measured relative viscosity vs shear rate for 40% suspensions of 106–125 μm glass spheres at $a/b = 0.0606$. The solid line represents a best fit linear model to the data.

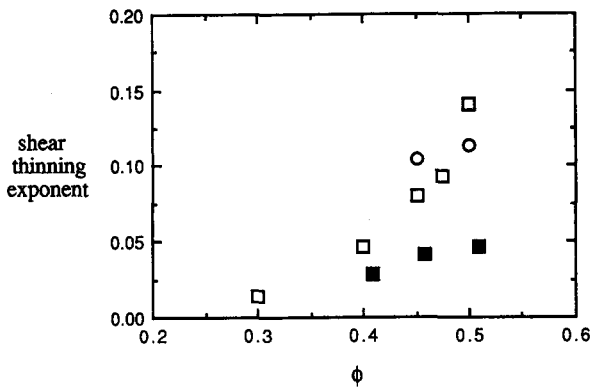

Figure 4. The shear thinning exponent vs concentration: □, 106–125 μm glass spheres; ■, 45–53 μm glass spheres; ○, 46 μm polystyrene spheres.

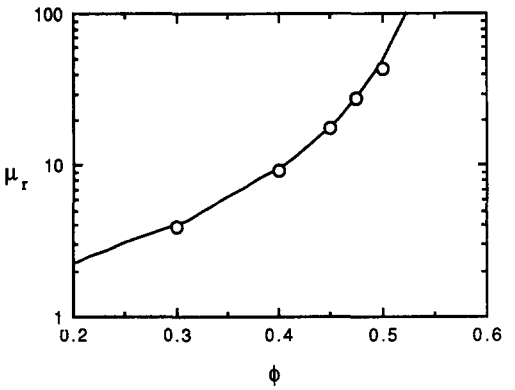

Figure 5. Relative viscosity vs concentration: ○, measured values for 106–125 μm glass spheres: ——, Eiler fit with $[\eta] = 3.18$, $\phi_{max} = 0.579$.

strain, however (figure 2), the characteristic strain to approach steady state for each type of experiment was similar, the remaining difference being a consequence of the non-linear dependence of the viscosity on the concentration gradient as described in section 2. Note that the solid curves in figure 2 are [19] and [21] fitted to the data, with best fit dimensionless diffusivities differing by only 8%.

4.2. Viscosity analysis

In order to calculate the diffusivity and hindered settling factor, it was necessary to develop a viscosity correlation for the suspensions studied. Shear thinning was present in all suspensions and was found to become stronger as the concentration was increased. It was also found to be more significant in the large glass sphere suspensions where, for a given change in shear rate, viscosities changed approximately twice as much as the viscosities of the small glass sphere suspensions. While the polystyrene sphere suspensions and the small glass sphere suspensions had particles of nearly equal size, the polystyrene suspensions were much more shear thinning. The shear thinning behavior was correlated by the power-law relationship:

$$\ln \mu_r = -n \ln \dot{\gamma} + \text{const.} \qquad [24]$$

The measured shear thinning behavior of large glass spheres at 40% for a particular value of a/b is given in figure 3. The shear thinning exponents n obtained for all suspensions studied are given

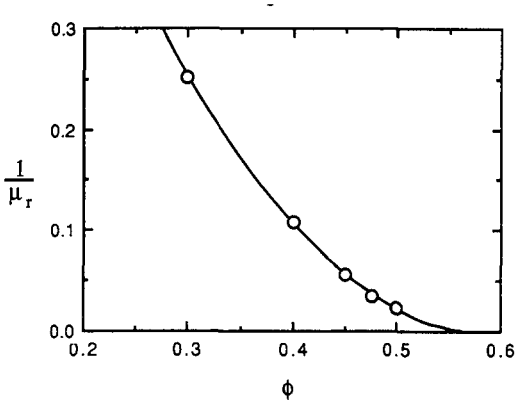

Figure 6. Value of $1/\mu_r$ vs concentration: ○, measured values for 106–125 μm glass spheres: ——, second-order fit.

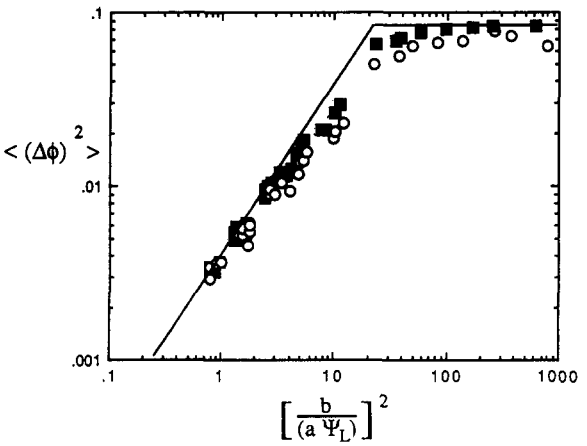

Figure 7. Mean square concentration deviation vs $[b/(a\Psi_L)]^2$ for 40% suspension of 106–125 μm glass spheres. The line of slope 2 represents theoretical expectations at high applied shear. The horizontal line represents the maximum value which would be measured for a fully settled layer: ○, step decrease in shear; ■, step increase in shear.

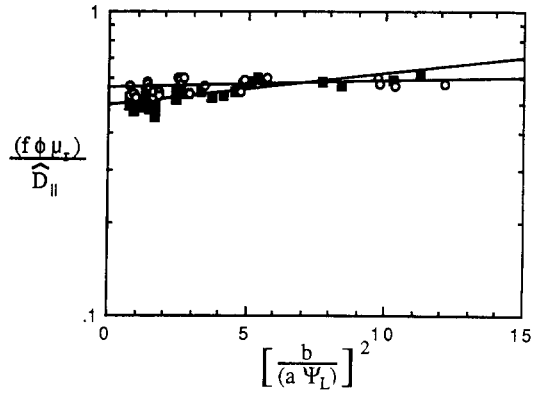

Figure 8. Measured values of $[(f\phi\mu_r)/\hat{D}_{||}]$ vs $[b/(a\Psi_L)]^2$ for 40% suspensions of 106–125 μm glass spheres: ○, step decrease in shear; ■, step increase in shear.

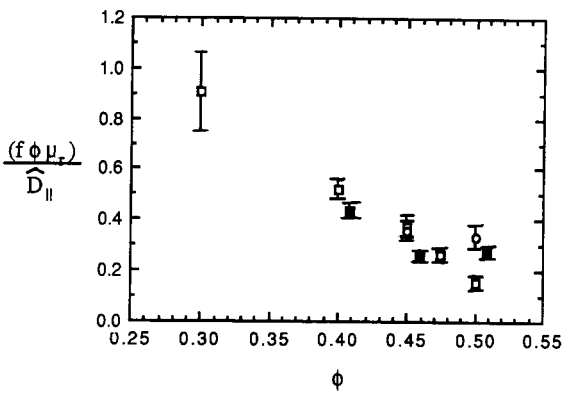

Figure 9. Measured values of $[(f\phi\mu_r)/\hat{D}_{||}]$ vs concentration: □, 106–125 μm glass spheres; ■, 45–53 μm glass spheres; ○, 46 μm polystyrene spheres. Error bars represent the scatter in the experimental observations.

in figure 4. Surprisingly, the viscosity was not found to be a strong function of the particle radius to half gap height ratio a/b, which was varied by changing the gap height for a given suspension. While most suspensions became slightly less viscous with decreasing a/b, the 45% large glass sphere suspensions exhibited the opposite behavior. The effect of gap height was much weaker than shear thinning and no systematic relationship could be determined because of the scatter in the experimental results.

A plot of the relative viscosity of the large glass sphere suspensions as a function of concentration at a shear rate of 24 s^{-1} is given in figure 5. Each data point in this figure is the interpolated value at each particular concentration of the viscosity using [24] fitted to all viscosity measurements. The 40% viscosity data point, for example, represents the average of 72 different measurements taken at shear rates ranging between ~5 and ~63 s^{-1} and a/b ratios ranging between 0.041 and 0.070. The viscosity of the large glass sphere suspensions for concentrations in the range 30–50% was found to be fit quite well by the modified Eiler equation:

$$\mu_r = \left(1 + \frac{\frac{1}{2}[\eta]\phi}{1 - \frac{\phi}{\phi_e}}\right)^2, \qquad [25]$$

where the intrinsic viscosity $[\eta] = 3.18$ and the empirical maximum concentration $\phi_e = 0.579$. These values are quite close to those of 3 and 0.58, respectively, reported by Leighton & Acrivos (1987b) for suspensions of 46 μm polystyrene spheres. Similar values were also found by Ogden & Davis (1990) for suspensions of 7.3 μm polystyrene latex spheres.

An important quantity in our calculations is the second derivative with respect to concentration of the reciprocal of the relative viscosity. From viscosities measured initially in step decrease experiments and at steady state in the step increase experiments for the large glass sphere suspensions, we found that $1/\mu_r$ is very well described by a quadratic function of concentration, as seen in figure 6, for a shear rate of 24 s^{-1}. This quadratic relationship appeared to hold at all shear rates used in our experiments. The second derivative of $1/\mu_r$ was found to be

$$\frac{1}{2}\frac{\partial^2\left(\frac{1}{\mu_r}\right)}{\partial\phi^2} = 3.57 - 0.165 \ln\dot{\gamma} \qquad [26]$$

for suspensions of large glass spheres with concentrations of 30–50%. Note that each of the 5 points in figures 5 and 6 represent information derived from 8–72 individual experiments. It is very difficult to extract a second derivative from experimental data, and the correlation given by [26] is likely to be accurate only at a concentration in the center of the range studied, e.g. at 40%. The use of [26] at 30 and 50% is likely to introduce significant errors in the calculation of the hindered settling function. Fitting the observed viscosity data to a cubic function of concentration suggests this error could be as great as 50%.

In the other two suspension systems there was not enough data to obtain a sufficiently accurate viscosity correlation to calculate a second derivative. As a consequence, the viscosity function of [26] obtained from the large glass sphere suspensions was employed in these systems. Note that this renders uncertain the calculations of the hindered settling factor for both the small glass and the polystyrene systems but has no effect on the calculated values of the effective diffusivity.

4.3. *Steady-state analysis*

From the measured initial and steady-state viscosities in a step increase experiment, the quantities α, δ and $\mu_{r,\bar{\phi}}$ were obtained with the use of [14] and [17]. In general, α was larger in experiments with smaller concentrations and/or smaller particle radius to gap height ratios and in those experiments with larger step changes in shear rate. In all of the suspensions, it was necessary to keep $\bar{\phi} + (\alpha + \delta)$ less than the concentration of a settled layer ϕ_{max}, and $\bar{\phi} - (\alpha + \delta) > 0$, in order for the calculated concentration profile to be physically realistic.

From [9], we can determine the ratio of the hindered settling factor to the effective diffusivity by examining the amplitude of the viscosity fluctuation as a function of the low shear Shields parameter. Figure 7 shows the mean square concentration deviation, $\langle(\Delta\phi)^2\rangle$, as determined from the observed viscosity fluctuation via [6] for the 40% large glass sphere suspensions. As expected from [9], this quantity is approximately proportional to $[b/(a\Psi_L)]^2$ for large Ψ_L. At lower Shields parameters, however, the deviation from the average concentration gradually falls away from this slope, suggesting that we are nearing experimental conditions where [9] does not apply. Indeed, as Ψ_L approaches zero, the concentration fluctuation approaches a maximum corresponding to a fully settled suspension in which all shearing occurs in the pure field above the settled bed. The limiting value for a settled bed is given by

$$\langle(\Delta\phi)^2\rangle = \frac{1}{2}\int_{-1}^{1} (\phi - \bar{\phi})^2 \, dy^* = \bar{\phi}(\phi_{max} - \bar{\phi}), \qquad [27]$$

where ϕ_{max} is the concentration of the settled layer. This limiting value is given by the horizontal line in figure 7 for a settled layer concentration of $\phi_{max} = 0.62$. Calculations of f and $\hat{D}_{\perp}$ for the experiments corresponding to this figure were done only when $[b/(a\Psi_L)]^2 < 12$.

Because the assumptions leading to [9] are valid in the limit of small concentration variations $\langle(\Delta\phi)^2\rangle$ which, in turn, vanish as $[b/(a\Psi_L)]^2$ becomes small, the value of $[(f\phi\mu_r)/\hat{D}_{\parallel}]$ for each suspension at a given concentration was determined by plotting $[(f\phi\mu_r)/\hat{D}_{\parallel}]$ vs $[b/(a\Psi_L)]^2$ and extrapolating to zero. An example of this for 40% large sphere suspensions is given in figure 8. We have plotted $[(f\phi\mu_r)/\hat{D}_{\perp}]$ vs ϕ in figure 9 for all suspensions studied except for the 20% large glass spheres. For this suspension the viscosity function $[\partial^2(1/\mu_r)/\partial\phi^2]$, necessary in calculating $[(f\phi\mu_r)/\hat{D}_{\parallel}]$, was not determined.

The error bars in figure 9, as well as those in figures 11 and 13, are a measure of the scatter in the data and not a measure of the error in the mean. Because of the large number of individual measurements made (more than 60 for the 40% large glass sphere experiments, for example), random errors in the extrapolated values of $[(f\phi\mu_r)/\hat{D}_{\parallel}]$, $\hat{D}_{\parallel}$ and f are negligible. Systematic error, such as polydispersity in particle size and shape, error in theory and the determination and use of the second deviative with respect to concentration of the reciprocal of the viscosity, is probably much larger than the random error but is difficult to quantify. The large quantity of time-dependent viscosity data obtained in these experiments is available in the thesis of Chapman (1991).

4.4. *Transient analysis*

The diffusivity was determined from transient viscosity measurements using [19] and [21]. As may be seen from examination of figure 2, these equations provided an excellent fit to the experimental data. The effective diffusivity measured by means of the model presented in section 2 will correspond to the diffusivity at the average concentration $\bar{\phi}$ only in the limit of small concentration variations in the gap. If we expand the diffusivity in a Taylor series about $\phi = \bar{\phi}$ we obtain the area average diffusivity in the gap to be

$$\langle\hat{D}_{\parallel}\rangle = \hat{D}_{\parallel}|_{\bar{\phi}} + \frac{1}{2}\left.\frac{\partial^2\hat{D}_{\parallel}}{\partial\phi^2}\right|_{\bar{\phi}} \langle(\Delta\phi)^2\rangle + O(\langle(\Delta\phi)^3\rangle), \qquad [28]$$

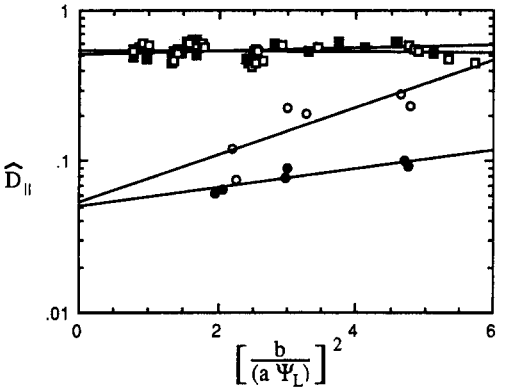

Figure 10. Measured effective diffusivity vs $[b/(a\Psi_L)]^2$ for 106–125 μm suspensions of glass spheres: ○, 20% step decrease in shear; ●, 20% step increase in shear; □, 40% step decrease in shear, ■, 40% step increase in shear.

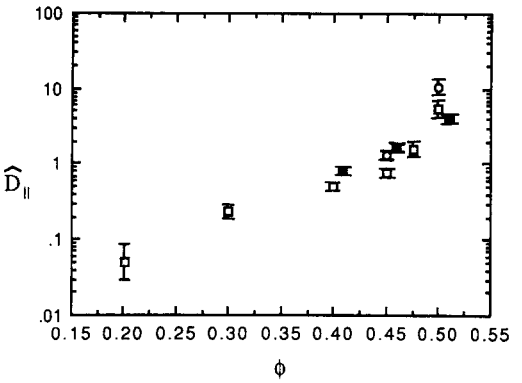

Figure 11. Measured effective diffusivity vs concentration: □, 106–125 μm glass spheres; ■, 45–53 μm glass spheres; ○, 46 μm polystyrene spheres. Error bars represent the scatter in the experimental observations.

since, as before, the average of $\Delta\phi$ across the gap is zero. Thus, the deviation between the measured average diffusivity and that corresponding to the average concentration should vanish as $\langle(\Delta\phi)^2\rangle$ becomes small. From [8] we find that $\langle(\Delta\phi)^2\rangle \sim [b/(a\Psi_L)]^2$, thus, as was the case for $[(f\phi\mu_r)/\hat{D}_{\|}]$, we may determine the diffusivity by plotting the measured diffusivity for each experiment as a function of $[b/(a\Psi_L)]^2$ and extrapolating to zero. This is shown for the 20 and 40% large glass sphere suspensions in figure 10.

For concentrations of 40–50%, the diffusivities of the large glass spheres slightly increased with increasing $[b/(a\Psi_L)]^2$ during step increase experiments and slightly decreased with increasing $[b/(a\Psi_L)]^2$ during step decrease experiments. In the 20 and 30% suspensions, however, the diffusivities increased strongly in the step decrease experiments. At these concentrations the settling velocities of the particles may have contributed to the measured effective diffusivity at the lower shear rates (e.g. the first term on the r.h.s. of [10] was not negligible, as had been assumed). This should be less significant for a step increase (as was indeed found experimentally) due to the higher diffusivity at the higher applied shear rate. In the small glass sphere suspensions and in the polystyrene sphere suspensions, there was very little variation in $\hat{D}_{\|}$ with increasing $[b/(a\Psi_L)]^2$ for step increase or step decrease experiments. Figure 11 shows the measured effective diffusivities (extrapolated to $[b/(a\Psi_L)]^2 = 0$) as a function of concentration in all systems studied. As expected, the diffusivities were very strongly dependent on concentration. In the large glass suspensions, the diffusivity increased by two orders of magnitude from a concentration of 20% to a concentration of 50%.

The effect of the particle diameter to gap height ratio on the effective diffusivity was also investigated. The extrapolated value of $\hat{D}_{\|}$ at $[b/(a\Psi_L)]^2 = 0$ for each value of a/b studied was plotted vs a/b for the 40% large glass sphere suspensions. While the diffusivity was observed to be a slightly decreasing function of a/b, the scatter in the data and the limited range of a/b used in our experiments prevented precise determination of the functional relation. From the data it appears that extrapolating the measured diffusivity to $a/b = 0$ would increase the value over that reported in figure 11 by no more than 10%.

The diffusivities of the small glass spheres were nearly twice as great as those of the large glass spheres at concentrations of 40 and 45%. At a concentration of 50%, however, the diffusivities were much closer. It appears that the discrepancies between the diffusivities of the different suspensions at 40 and 45% cannot be accounted for by experimental error. The spheres used in both the large glass sphere and small glass sphere suspensions were made by the same manufacturer and the dimensionless breadth of the particle size distribution in both suspensions were similar, thus the discrepancy is somewhat puzzling.

Other suspension properties such as the importance of van der Waals and electroviscous forces depend on the absolute particle size, however, and thus will be different in the two types of suspensions. Smart & Leighton (1989) also demonstrated that the absolute magnitude of the surface roughness of these sizes of glass spheres was the same, and thus the dimensionless roughness

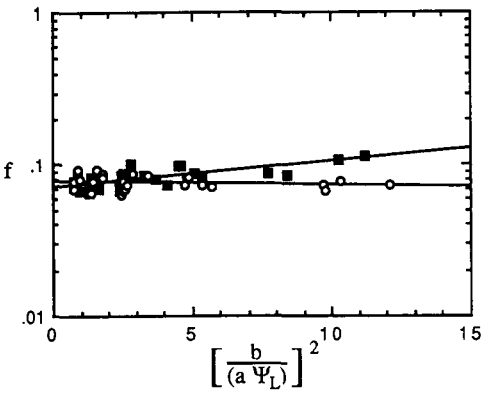

Figure 12. Measured hindered settling factor vs $[b/(a\Psi_L)]^2$ for 40% suspension of 106–125 μm glass spheres: ○, step decrease in shear; ■, step increase in shear.

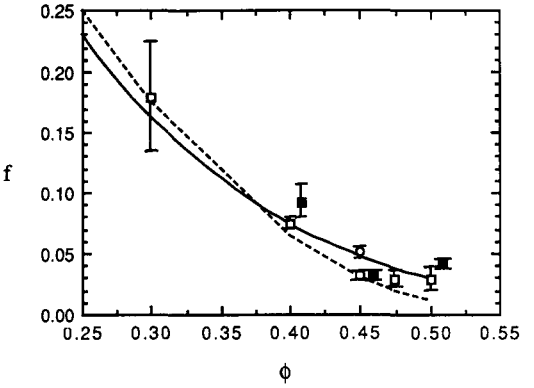

Figure 13. Measured hindered settling factor vs concentration: □, 106–125 μm glass spheres; ■, 45–53 μm glass spheres; ○, 46 μm polystyrene spheres; ——, Richardson–Zaki correlation; – – –, correlation used by Leighton & Acrivos (1986). Error bars represent the scatter in the experimental observations.

increases as the particle diameter decreases. We may expect that the diffusivity is more sensitive to the suspension structure or particle distribution than other suspension properties such as the viscosity, since it is proportional to a^2 and hence would be directly affected by any aggregation in the suspension. Explanation of the causes of this discrepancy must remain the subject of future investigations.

While the polystyrene spheres were found to exhibit diffusivities much like the similar-sized small glass spheres, there was a significant amount of scatter in $\hat{D}_{\parallel}$, particularly in the 50% suspensions. It is therefore difficult to make a complete comparison between particle materials. A comparison of the diffusivities with previous results found in the literature is presented in the next section.

From [23] the hindered settling factor f can be determined for each experiment. Similar to the diffusivity calculation, the value of f reported for each suspension was found by plotting the calculated hindered settling factor for each experiment as a function of $[b/(a\Psi_L)]^2$ and then extrapolating to zero as is shown in figure 12 for 40% large glass sphere suspensions. Figure 13 shows the relationship for f as a function of ϕ for each suspension studied except the 20% large glass sphere suspensions. As expected, f is a decreasing function of concentration and our results show good agreement with the Richardson–Zaki correlation (Davis & Acrivos 1985) for an unsheared suspension:

$$f = (1 - \phi)^{5.1}. \qquad [29]$$

While we would expect the hindered settling function to depend on the local particle distribution and hence to be different in sheared and unsheared suspensions, our measurements are in qualitative agreement with those of Lynch (1985) for sedimentation normal to the plane of shear. In that study, it was observed that the hindered settling function increased in dilute suspensions as they were sheared in a plane normal to the direction of sedimentation. The difference between sheared and unsheared systems decreased with increasing concentration, however, and was not measurable for concentrations between 15 and 25%, the highest concentration used in that study.

In their study of viscous resuspension, Leighton & Acrivos (1986) assumed that $f\mu_r = 1 - \phi$. This is equivalent to assuming that the spheres settle through an effective medium with the density of the suspension (rather than the pure fluid) and with a viscosity identical to the suspension shear viscosity. As may be seen in figure 13, this substantially underestimates f at higher concentrations. It must be emphasized that since the value of the hindered settling factor calculated from our experiments is proportional to the second derivative of the reciprocal of the relative viscosity, the estimated values are quite uncertain. Direct concentration profile measurements are necessary to determine if the hindered settling factor differs between sheared and unsheared suspensions, however such measurements are beyond current experimental techniques at these concentrations and particle sizes.

5. DISCUSSION

It is interesting at this point to discuss the mechanism by which effective diffusion occurs. While it has recently been shown that drift may arise from purely hydrodynamic interactions (Koch 1990), Leighton & Acrivos (1987b) suggested that the source of particle drift within the plane of shear could be described in terms of irreversible interactions between particles as the suspension is sheared. According to their model, the presence of gradients in concentration lead to gradients in viscosity which, in turn, cause particles undergoing irreversible interactions to be displaced from regions of high viscosity to low viscosity and hence from high concentration to low. They, thus, suggested that the effective diffusivity scale as

$$D_{\perp} = K_{\parallel} \frac{\phi^2}{\mu} \frac{d\mu}{d\phi} \dot{\gamma} a^2, \qquad [30]$$

where $K_{\parallel}$ was expected to be a function of concentration because of the dependence of the geometry of particle interactions on suspensions microstructure, and in particular on the degree of aggregation. The authors reported $K_{\perp}$ to be a moderate function of concentration with a value of 0.6 at a concentration of 45%, although their experiments lacked sufficient accuracy to test the model.

We may use the results of our large glass sphere experiments to provide a better test of this model. Figure 14 shows the correlation [30] with a best fit value of $K_{\parallel} = 0.33$ for these suspensions. We find from figure 14 that the model adequately describes the behavior of the large glass sphere suspensions (□) for concentrations between $0.2 < \phi < 0.45$, however at higher concentrations the diffusivity appears to increase more rapidly than predicted by [30]. The discrepancy is possibly due to the formation of large aggregates at higher concentrations, thus increasing the length scale of the particle interactions. Further experiments at higher concentrations are necessary to resolve this issue, however.

Figure 14 also compares the diffusivity measured by Leighton & Acrivos (1987b) with those reported here. Our measurements are in close agreement at concentrations of 40–50% considering the scatter in the earlier experiments. It should be noted that our technique provided much more reproducible results because we could control and vary the magnitude of the concentration gradient. We were also able to study a wider range of concentrations and perform experiments at a larger number of different particle diameter to gap height ratios and shear rates.

Surprisingly, the correlation proposed by Leighton & Acrivos (1986) in the viscous resuspension study (—— in figure 14),

$$\hat{D} = \tfrac{1}{3}\phi^2(1 + \tfrac{1}{2}e^{8.8\phi}), \qquad [31]$$

does a reasonable job of describing our measurements, even at fairly low concentrations. Equation [31] was developed by combining the measured effective diffusivity at high concentrations (Leighton

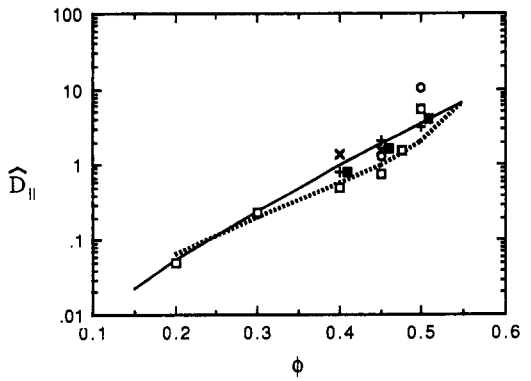

Figure 14. Comparison of the diffusion coefficient vs concentration with the correlation proposed by Leighton & Acrivos (1986): □, 106–125 μm glass spheres; ■, 45–53 μm glass spheres; ○, 46 μm polystyrene spheres; +, 46 μm polystyrene spheres (Leighton & Acrivos 1987b); ×, 86 μm polystyrene spheres (Leighton & Acrivos 1987b); ——, Leighton & Acrivos (1986) correlation; ----, Leighton & Acrivos (1987b) correlation with $K_{\parallel} = 0.33$.

& Acrivos 1987b) with the measured coefficient of self-diffusion for dilute suspensions (Leighton & Acrivos 1987a) into a smooth curve. As a consequence, the correlation involved no measurements of the effective diffusivity at concentrations $<40\%$. From figure 14, however, it appears that the diffusivity at 50% increases much more rapidly with concentration than the correlation and hence [31] is of little use beyond this point. A more accurate correlation cannot be developed until we better understand the behavior at concentrations approaching the maximum packing fraction.

Acknowledgements—We would like to acknowledge the donation of the Carri-Med Controlled Stress Rheometer used in this work by Mitech Corp. This work was supported in part by the American Chemical Society Petroleum Research Fund and the National Science Foundation.

REFERENCES

Bossis, G. & Brady, J. F. 1987 Self-diffusion of Brownian particles in concentrated suspensions under shear. *J. Chem. Phys.* **87,** 5437–5448.

Chapman, B. K. 1991 Shear-induced gradient diffusion in concentrated suspensions of noncolloidal spheres. Ph.D. Thesis, Univ. of Notre Dame, Ind.

Davis, R. H. & Acrivos, A. 1985 Sedimentation of noncolloidal particles at low Reynolds numbers. *A. Rev. Fluid Mech.* **17,** 91–118.

Davis, R. H. & Leighton, D. T. 1987 Shear-induced transport of a particle layer along a porous wall. *Chem. Engng Sci.* **42,** 275–281.

Eckstein, E. C., Bailey, D. G. & Shapiro, A. H. 1977 Self-diffusion of particles in shear flow of a suspension. *J. Fluid Mech.* **79,** 191.

Gadala-Maria, F. A. 1979 The rheology of concentrated suspensions. Ph.D. Thesis, Stanford Univ., Calif.

Ho, B. P. & Leal, L. G. 1974 Inertial migration of rigid spheres in two-dimensional unidirectional flows. *J. Fluid Mech.* **65,** 365–400.

Koch, D. L. 1989 On hydrodynamic diffusion and drift in sheared suspensions. *Phys. Fluids* **A1,** 1742–1745.

Leighton, D. & Acrivos, A. 1986 Viscous resuspension. *Chem. Engng Sci.* **41,** 1377–1384.

Leighton, D. & Acrivos, A. 1987a Measurement of shear-induced self-diffusion in concentrated suspensions of spheres. *J. Fluid Mech.* **177,** 109–131.

Leighton, D. & Acrivos, A. 1987b The shear-induced migration of particles in concentrated suspensions. *J. Fluid Mech.* **181,** 415–439.

Lynch, E. D. 1985 Sedimentation in quiescent and sheared suspensions. Ph.D. Thesis, California Institute of Technology, Pasadena, Calif.

Ogden, G. E. & Davis, R. H. 1990 Experimental determination of the permeability and relative viscosity for fine latexes and yeast suspensions. *Chem. Engng Commun.* **91,** 11–28.

Schaflinger, U., Acrivos, A. & Zhang, K. 1990 Viscous resuspension of a sediment within a laminar and stratified flow. *Int. J. Multiphase Flow* **16,** 567–578.

Segre, G. & Silberberg, A. 1962 Behaviour of macroscopic rigid spheres in Poiseuille flow. Part 1. Determination of local concentration by statistical analysis of particle passages through crossed light beams. *J. Fluid Mech.* **14,** 115–135.

Segre, G. & Silberberg, A. 1962 Behaviour of macroscopic rigid spheres in Poiseuille flow. Part 2. Experimental results and interpretation. *J. Fluid Mech.* **14,** 136–157.

Smart, J. R. & Leighton, D. T. 1989 Measurement of the hydrodynamic surface roughness of noncolloidal spheres. *Phys. Fluids* **A1,** 52–60.

Thomas, D. G. 1961 Transport characteristics of suspensions: II. Minimum transport velocity for fluocculated suspensions in horizontal pipes. *AIChE Jl* **7,** 423–430.